

# Temperature-Controlled Optical Activity and Negative Refractive Index

Meng Liu, Eric Plum,\* Hua Li, Shaoxian Li, Quan Xu, Xueqian Zhang, Caihong Zhang, Chongwen Zou, Biaobing Jin, Jianguang Han,\* and Weili Zhang\*

Chiral media exhibit optical activity, which manifests itself as differential retardation and attenuation of circularly polarized electromagnetic waves of opposite handedness. This effect can be described by different refractive indices for left- and right-handed waves and yields a negative index in extreme cases. Here, active control of chirality, optical activity, and refractive index is demonstrated. These phenomena are observed in a terahertz metamaterial based on 3D-chiral metallic resonators and achiral vanadium dioxide inclusions. The chiral structure exhibits pronounced optical activity and a negative refractive index at room temperature when vanadium dioxide is in its insulating phase. Upon heating, the insulator-to-metal phase transition of vanadium dioxide effectively renders the structure achiral, resulting in absence of optical activity and a positive refractive index. The origin of the structure's chiral response is traced to magnetic coupling between front and back of the structure, whereas the temperature-controlled chiral-to-achiral transition is found to correspond to a transition from magnetic to electric dipole excitations. The use of a four-fold rotationally symmetric design avoids linear birefringence and dichroism, allowing such a structure to operate as tunable polarization rotator, adjustable linear polarization converter, and switchable circular polarizer.

refractive indices for left- and right-handed circularly polarized electromagnetic waves, resulting in polarization rotation (circular birefringence) and preferential absorption of one circular polarization (circular dichroism). Since then, it has been discovered that optical activity can be influenced by temperature,<sup>[3,4]</sup> magnetic field,<sup>[5]</sup> electric field,<sup>[6,7]</sup> and light intensity.<sup>[8]</sup> However, optical activity is weak in natural materials, requiring interaction lengths that are large in comparison to the wavelength to accumulate significant polarization changes. This is especially true at THz frequencies owing to the large mismatch of THz wavelengths (hundreds of micrometers) and characteristic dimensions of crystal lattices and molecules (about a nanometer). Changes of optical activity in response to temperature, fields, or light intensity can reach the same order of magnitude as optical activity when phase transitions are involved, but typically they are orders of magnitude weaker,

i.e., negligible. Much larger optical activity can be engineered in metamaterials as the characteristic dimensions of such artificial materials can be chosen to be comparable to the wavelength of the radiation of interest.<sup>[9–14]</sup> In some cases, circular birefringence has been sufficiently large to achieve a negative refractive index for one circular polarization or the other.<sup>[15,16]</sup>

## 1. Introduction

Over two centuries ago, François Arago discovered that quartz possesses the ability to rotate the polarization state of light.<sup>[1]</sup> Within a few decades, Louis Pasteur linked this effect of optical activity to chirality.<sup>[2]</sup> Optical activity corresponds to different

Dr. M. Liu, Dr. S.-X. Li, Dr. Q. Xu, Dr. X.-Q. Zhang, Prof. J.-G. Han  
Center for Terahertz Waves and College of Precision Instrument and  
Optoelectronics Engineering  
Tianjin University  
Tianjin 300072, China  
E-mail: jiaaghan@tju.edu.cn

Dr. M. Liu  
College of Electronic and Information Engineering  
Shandong University of Science and Technology  
Qingdao 266590, P. R. China

 The ORCID identification number(s) for the author(s) of this article can be found under <https://doi.org/10.1002/adfm.202010249>.

© 2021 The Authors. Advanced Functional Materials published by Wiley-VCH GmbH. This is an open access article under the terms of the Creative Commons Attribution License, which permits use, distribution and reproduction in any medium, provided the original work is properly cited.

DOI: 10.1002/adfm.202010249

Dr. E. Plum  
Centre for Photonic Metamaterials and Optoelectronics Research Centre  
Zepler Institute  
University of Southampton  
Southampton SO17 1BJ, UK  
E-mail: erp@orc.soton.ac.uk

H. Li, Prof. C.-H. Zhang, Prof. B.-B. Jin  
Research Institute of Superconductor Electronics (RISE)  
School of Electronic Science and Engineering  
Nanjing University  
Nanjing 210093, P. R. China

Prof. C.-W. Zou  
National Synchrotron Radiation Laboratory  
University of Science and Technology of China  
Hefei 230029, P. R. China

Prof. W.-L. Zhang  
School of Electrical and Computer Engineering  
Oklahoma State University  
Stillwater, OK 74078, USA  
E-mail: weili.zhang@okstate.edu

Electromechanically reconfigurable metamaterials have enabled substantial electric control over optical activity,<sup>[17–21]</sup> while phase transitions in THz metamaterials have enabled control over the related phenomena of asymmetric transmission<sup>[22]</sup> and chiral mirrors.<sup>[23]</sup>

Here, we demonstrate temperature-controlled chirality, optical activity, and index of refraction. Switching between effectively chiral and achiral structures is achieved by exploiting the insulator-to-metal phase transition of vanadium dioxide in a THz metamaterial. At room temperature, the metamaterial is an array of mutually twisted metallic split rings in parallel planes, exhibiting large circular birefringence, circular dichroism, and a negative index of refraction. Upon heating above the phase transition temperature, vanadium dioxide gradually short-circuits the gaps of the rings, resulting in an effectively achiral structure with negligible optical activity and positive refractive index. In its chiral state, optical activity is associated with magnetic resonant modes and magnetic coupling of the split rings, while in its achiral state, the metamaterial exhibits an electric dipole response. The overall structure has fourfold rotational symmetry, which avoids linear birefringence and dichroism, allowing such metamaterials to operate as temperature-controlled polarization rotator, linear polarization converter, and circular polarizer.

## 2. Design and Characterization

The temperature-controlled 3D-chiral metamaterial is shown by **Figure 1**. It is based on pairs of metallic split ring resonators (SRRs) separated by a dielectric spacer. Looking along +z,

3D chirality arises from a 90° clockwise rotation of the back SRRs relative to the corresponding front SRRs (Figure 1a). Four such split ring pairs are combined to form a fourfold rotationally symmetric unit cell that ensures an isotropic response to normally incident radiation because of absence of in-plane preferred directions (Figure 1b). Temperature control of the metamaterial is enabled by placing each SRR pair in between a pair of matching continuous vanadium dioxide (VO<sub>2</sub>) rings, such that the heating-induced dielectric-to-metal phase transition of VO<sub>2</sub> short-circuits the gap of each SRR. This phase transition of VO<sub>2</sub> occurs at a characteristic temperature of 65–68 °C and is accompanied by a drastic change in conductivity exceeding four orders of magnitude.<sup>[24–26]</sup> Thus, heating transforms the 3D-chiral metamaterial into an effectively achiral structure.

To fabricate the structure, identical arrays of 150-nm-thick VO<sub>2</sub> square rings were patterned on two sapphire substrates by optical lithography and plasma etching (CF<sub>4</sub>/O<sub>2</sub>). In a second lithography step, a gold SSR of 200 nm thickness was formed on top of each VO<sub>2</sub> ring by gold deposition, patterning, and lift-off (Figure 1c). Then the metamaterial was assembled by stacking the two structurally identical components with the SRRs facing each other and spaced by a lossy polyimide slab of 33 μm thickness. The metamaterial has a size of 1 cm × 1 cm and a square period of 135 μm.

The spectral response of this metamaterial was optimized by parametric analysis using CST Microwave Studio. Taking advantage of structure's periodicity, we modeled a single unit cell with periodic boundary conditions in the lateral directions. Open boundary conditions were applied in the propagation direction. The different materials were described by a conductivity of  $3.56 \times 10^7 \text{ S m}^{-1}$  for gold, a dielectric constant of 9.67

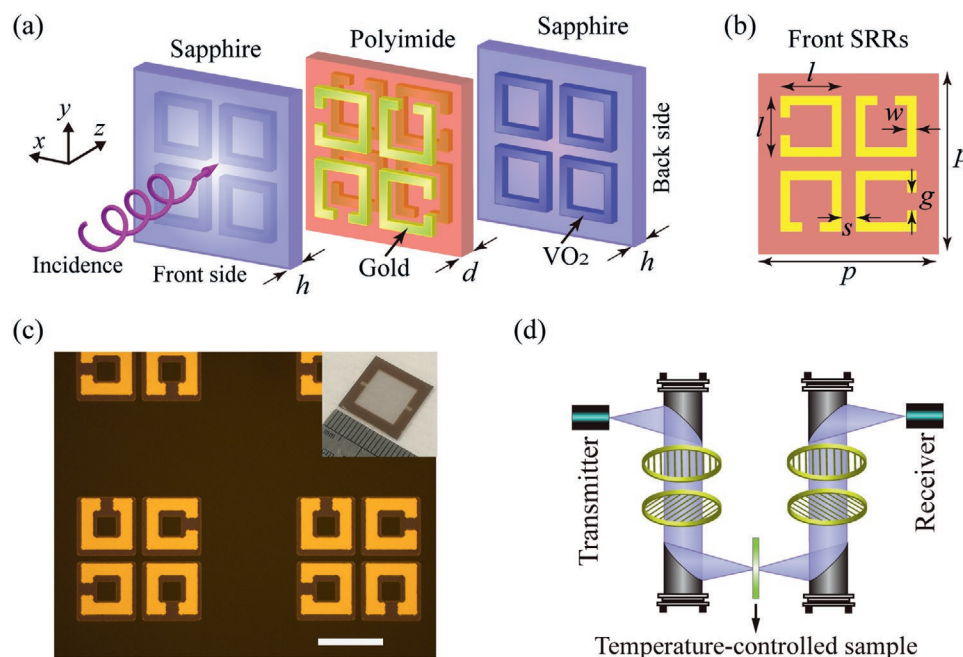


**Figure 1.** Metamaterial with switchable chirality. a) Unit cell, composed of pairs of identical and mutually twisted gold SRRs in parallel planes sandwiched in between square VO<sub>2</sub> rings with geometrical parameters  $h = 1000 \mu\text{m}$ ,  $d = 33 \mu\text{m}$ ,  $l = 33 \mu\text{m}$ ,  $w = 9 \mu\text{m}$ ,  $p = 135 \mu\text{m}$ ,  $g = 6 \mu\text{m}$ , and  $s = 7 \mu\text{m}$ . All layers are placed directly on top of each other. b) SRR layer of the unit cell, containing SRRs rotated in 90° steps to achieve an isotropic response. c) Optical microscope image of gold SRRs and VO<sub>2</sub> square rings with a 40 μm scale bar. The inset shows a photo of the whole sample. d) Sample characterization by THz-TDS.

for sapphire, and a dielectric constant of 2.93 with loss tangent delta of 0.044 for polyimide. VO<sub>2</sub> was modeled with conductivities ranging from 10<sup>[24]</sup> to 2.6 × 10<sup>5</sup> S m<sup>-1</sup>,<sup>[24,27,28]</sup> corresponding to its insulating and metallic phases, respectively.

The chiral metamaterial was characterized by THz time-domain spectroscopy (THz-TDS). The transmission coefficients of the fabricated metamaterial were measured for the normally incident THz waves (along +z) at temperatures ranging from 23 to 102 °C. Within the THz-TDS setup, a mode-locked laser centered at 780 nm wavelength with 35 fs pulse duration and 78 MHz repetition rate is split into equal intensity beams (with 10 mW average power). Each beam is then focused on the surface of a different photoconductive antenna. One beam is used to generate the THz transient by excitation of a biased photoconductive antenna, while the other acts as a gate in a photoconductive receiver to detect the THz pulse coherently. The temporal shape of the THz transient is recorded by gradually changing the relative delay between THz transient and gate pulse while monitoring the current induced in the external circuitry by the THz field. The signal-to-noise ratio of the THz-TDS system exceeds 5000:1 in the experimental frequency range of 0.4–1.0 THz. Fabricated samples are fixed to an electrically controlled heater which has an aperture at its center. Transmission measurements are performed in a drying chamber and four polarizers are used to select and transform THz polarizations as only horizontally polarized THz waves are

efficiently radiated and detected in this THz-TDS system. All presented THz transmission measurements were normalized to spectra of a sample without gold and without VO<sub>2</sub> structures. Transmission characteristics for circularly polarized waves were determined by transformation from the linear polarization basis to the circular polarization basis as described in ref. [22].

### 3. Results and Discussion

The transmission characteristics of the metamaterial, as it transitions from its room temperature chiral state to its high temperature achiral state, were simulated and measured. The metamaterial's chiral state, which has insulating SRR gaps, is modeled with a VO<sub>2</sub> conductivity of 10 S m<sup>-1</sup> and measured at room temperature. The phase transition is studied by increasing the metamaterial temperature and simulated by increasing the conductivity of VO<sub>2</sub>, which effectively eliminates the chirality of the structure by gradually short-circuiting the SRR gaps. The effectively achiral state is measured at the maximum accessible temperature of 102 °C and modeled with a VO<sub>2</sub> conductivity of 2.6 × 10<sup>5</sup> S m<sup>-1</sup>.

Figure 2 shows the metamaterial's temperature-dependent transmittance spectra for THz waves of left-handed circular polarization (LCP, shown left) and right-handed circular polarization (RCP, shown right) according to simulations (top) and measurements (bottom). Here, we define RCP (+) as clockwise

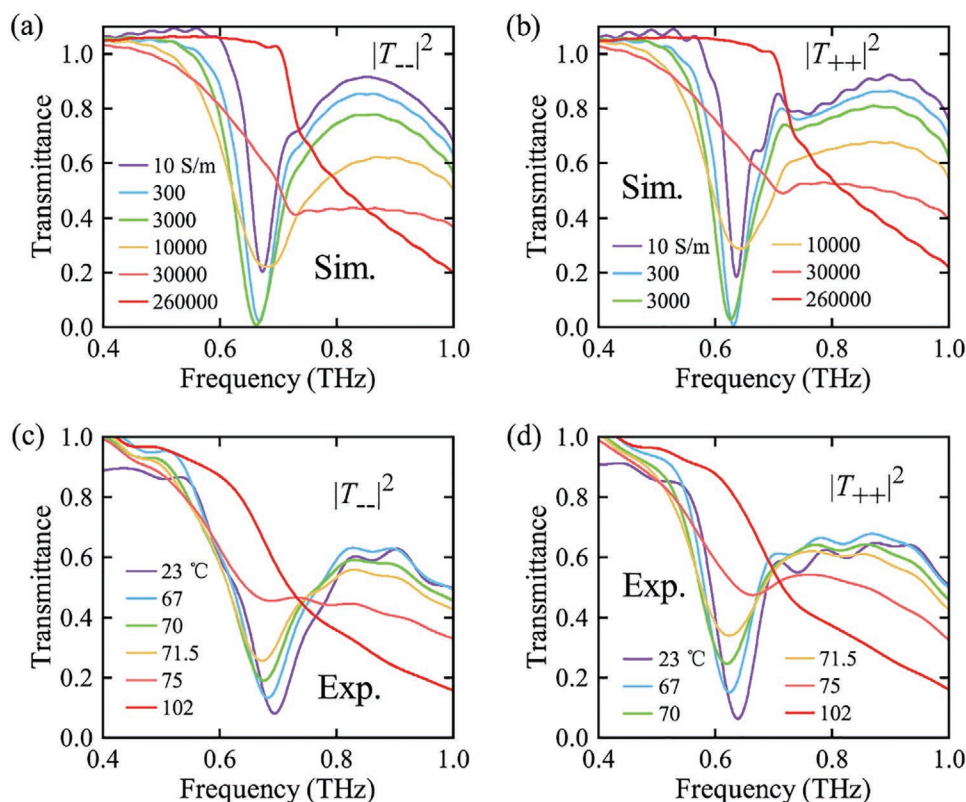
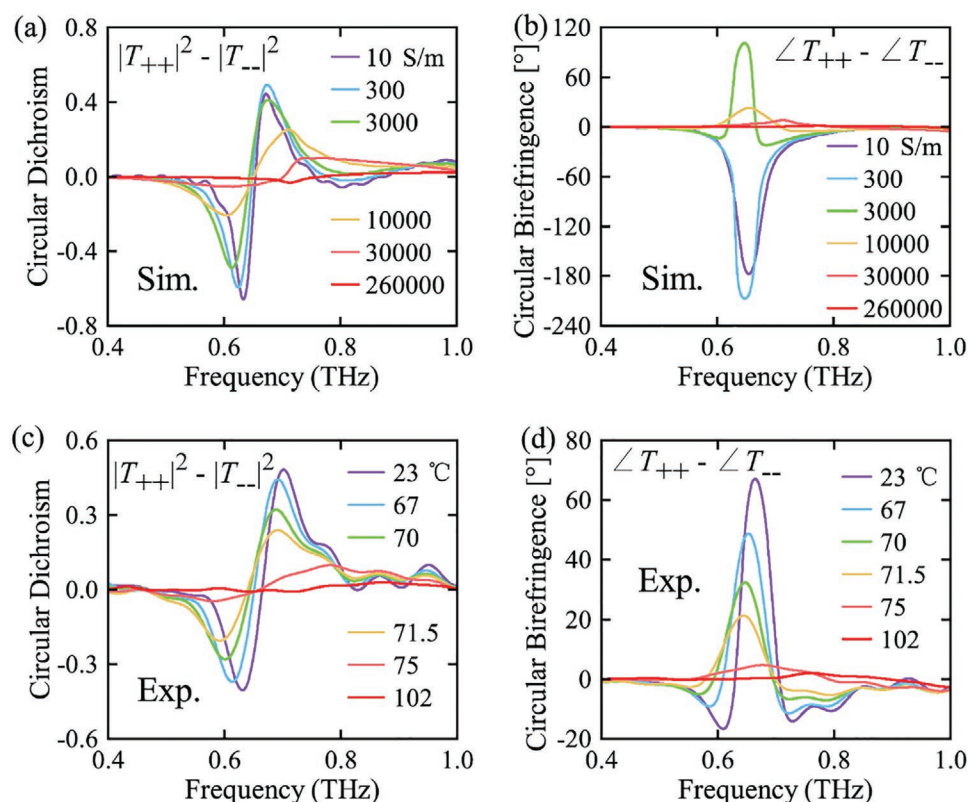


**Figure 2.** Switching of the transmittance for circularly polarized waves as the VO<sub>2</sub> phase transitions from insulating to metallic. a,b) Simulated frequency dependence of copolarized transmittance for LCP (–) and RCP (+) for VO<sub>2</sub> conductivities ranging from 10 to 2.6 × 10<sup>5</sup> S m<sup>-1</sup>. c,d) Measured frequency dependence of copolarized transmittance for LCP and RCP at temperatures ranging from 23 to 102 °C.  $|T_{ij}|^2$  represents the *i*-polarized transmittance of the sample resulting from *j*-polarized illumination.  $|T_{++}|^2$  and  $|T_{+-}|^2$  are negligible in all cases.

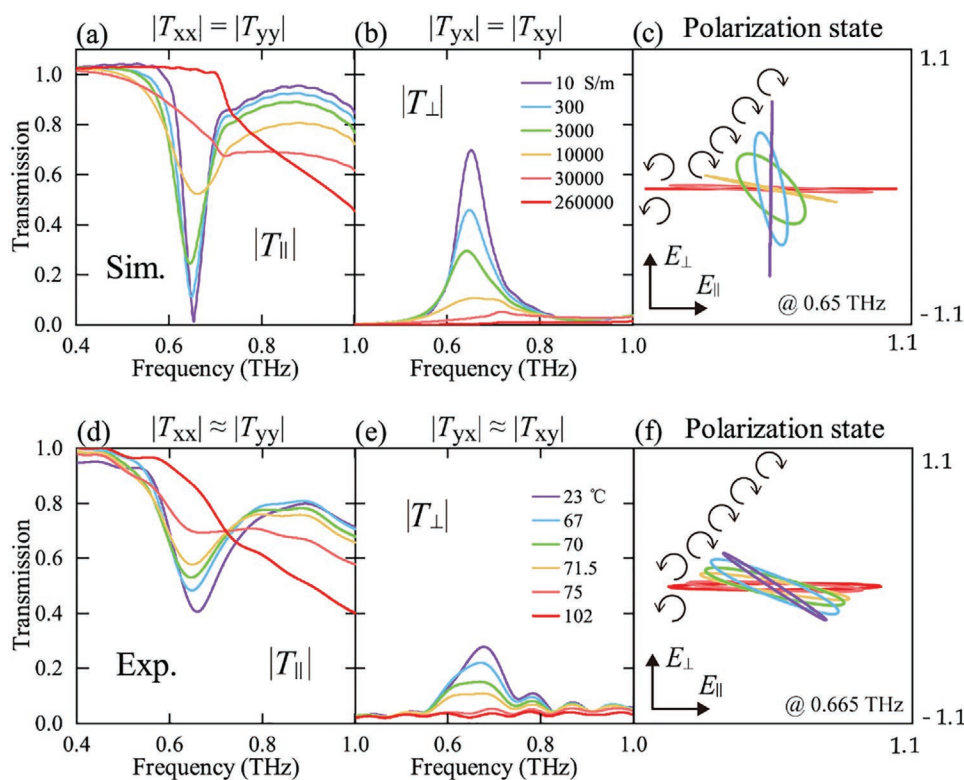
rotation of the electric field at a fixed position as seen by an observer looking into the THz beam toward the source.  $|T_{ij}|^2$  represents the  $i$ -polarized transmittance of the sample resulting from the  $j$ -polarized illumination.  $T_{ij}$  is the corresponding field transmission coefficient, relating transmitted and incident electric fields according to  $E_i^{\text{trans}} = T_{ij} E_j^{\text{inc}}$ . Circular polarization conversion cannot occur at normal incidence owing to the structure's isotropic (fourfold rotationally symmetric) design, and indeed  $|T_{+-}|^2$  and  $|T_{-+}|^2$  are zero within numerical and experimental accuracy in all cases. It follows that the structure can be described in terms of circularly polarized eigenstates. The metamaterial's co-polarized transmittance spectra are strongly dependent on temperature ( $\text{VO}_2$  conductivity). At room temperature ( $10 \text{ S m}^{-1}$ ), the spectral dependencies of  $|T_{-}|^2$  and  $|T_{++}|^2$  are different from each other, exhibiting a pronounced resonance just above and just below  $0.65 \text{ THz}$ , respectively. The difference between  $|T_{-}|^2$  and  $|T_{++}|^2$  reveals the presence of circular dichroism, i.e., chirality of the metamaterial response at room temperature. As the metamaterial is heated above the dielectric-to-metal phase transition of  $\text{VO}_2$  to  $102 \text{ }^\circ\text{C}$  ( $2.6 \times 10^5 \text{ S m}^{-1}$ ), the resonances vanish and  $|T_{-}|^2$  and  $|T_{++}|^2$  become (almost) identical, which is consistent with the expected achiral metamaterial response at high temperatures. The observed behavior corresponds to a thermally switchable notch filter exhibiting different low-temperature stop bands for LCP and RCP, which are separated by  $0.035$  and  $0.065 \text{ THz}$  according to simulations and experiments, respectively.

Figure 3 illustrates the active thermal control over the metamaterial's chiral response in terms of the manifestations of optical activity: circular dichroism (differential transmittance of circularly polarized waves,  $|T_{++}|^2 - |T_{-}|^2$ ) and circular birefringence (differential retardation of circularly polarized waves,  $\angle T_{++} - \angle T_{-}$ ). When the metamaterial is in its chiral state, i.e., at low temperatures (low  $\text{VO}_2$  conductivity), strong circular dichroism and circular birefringence are associated with the resonance around  $0.65 \text{ THz}$ . As the structure is heated, its optical activity reduces gradually and dramatically in the  $67\text{--}75 \text{ }^\circ\text{C}$  temperature range, i.e., around the dielectric-to-metal phase transition temperature of  $\text{VO}_2$ . At higher temperatures (i.e., at high  $\text{VO}_2$  conductivity), the chiral response vanishes almost entirely, i.e., circular dichroism and birefringence become negligible. Thus, the metamaterial is a thermally tunable optically active element. At selected frequencies and room temperature, the structure acts as circular polarizer, with an experimentally observed polarization contrast  $|T_{-}|^2 / |T_{++}|^2$  reaching up to  $78$ . At the maximum of circular birefringence, which coincides with vanishing circular dichroism, the device acts as polarization rotator, with experimentally observed polarization rotation of up to  $33.5^\circ$  (half of the circular birefringence). Both functions, circular polarizer and polarization rotator, can be switched off by heating the device to a temperature well-above the dielectric-to-metal phase transition temperature of  $\text{VO}_2$ .

Active control of the metamaterial's optical activity also manifests in its transmission characteristics for linearly polarized



**Figure 3.** Switching of optical activity as  $\text{VO}_2$  transitions from insulating to metallic. Simulated frequency dependence of a) circular dichroism and b) circular birefringence for  $\text{VO}_2$  conductivities  $\sigma$  ranging from  $10$  to  $2.6 \times 10^5 \text{ S m}^{-1}$ . Measured frequency dependence of c) circular dichroism and d) circular birefringence at temperatures ranging from  $23$  to  $102 \text{ }^\circ\text{C}$ .



**Figure 4.** Switching of linear polarization conversion as VO<sub>2</sub> transitions from insulating to metallic. Simulated frequency dependence of the a) co- and b) cross-polarized transmission amplitudes for linearly polarized waves for VO<sub>2</sub> conductivities ranging from 10 to  $2.6 \times 10^5$  S m<sup>-1</sup>. c) Transmitted polarization state at 0.65 THz for incident linearly polarized waves. Measured frequency dependence of the d) co- and e) cross-polarized transmission amplitudes for linearly polarized waves at temperatures ranging from 23 to 102 °C. f) Transmitted polarization state at 0.665 THz for incident linear polarization. Polarization ellipses are shown as seen by an observer looking from the receiver at the source.

THz waves, see **Figure 4**. Owing to its fourfold rotational symmetry, the metamaterial properties are the same for normally incident waves of  $x$ ,  $y$  or any other linear polarization. Therefore, the metamaterial can be characterized by transmission amplitudes for incident and transmitted waves with either parallel or orthogonal linear polarizations,  $|T_{\parallel}|$  and  $|T_{\perp}|$ . (Indeed,  $|T_{\parallel}| = |T_{xx}| = |T_{yy}|$  and  $|T_{\perp}| = |T_{yx}| = |T_{xy}|$  within numerical and experimental accuracy.) At room temperature (low VO<sub>2</sub> conductivity), the metamaterial's resonance is associated with a minimum of co-polarized transmission  $|T_{\parallel}|$  and a maximum of cross-polarized transmission  $|T_{\perp}|$ . The latter arises from substantial rotation of the transmitted polarization state (circular birefringence), and in case of elliptical polarization of the transmitted wave also from circular dichroism. Upon heating, the metamaterial's resonant and chiral response weakens dramatically in the temperature window of 67–75 °C, resulting in negligible polarization changes at higher temperatures. Thus, the metamaterial allows active polarization control and can be used to convert a tunable fraction of a linearly polarized incident THz wave to the orthogonal polarization state.

To reveal the microscopic origin of the metamaterial's chiral and achiral responses at low and high temperatures, we simulated the modes excited by  $x$ -polarized illumination at 0.65 THz, see **Figure 5**. The surface current oscillations are revealed by magnetic field perpendicular to the SRR planes, which arises from current oscillations within SRRs according to Ampère's law.

Our simulations reveal two types of current distributions, magnetic and electric dipole modes,  $\mathbf{m}$  and  $\mathbf{d}$ , as shown in Figure 5.

The origin of the metamaterial's chiral response at low temperatures (10 S m<sup>-1</sup> VO<sub>2</sub> conductivity) can be understood by considering how the magnetic dipole modes cause linear polarization conversion. Strong, resonant magnetic dipole modes are excited when the incident electric field is parallel to the middle of an SRR wire (e.g., SRRs 1<sup>f</sup> and 2<sup>b</sup>). They are looped LC charge oscillations on the SRR that correspond to a magnetic moment oscillating perpendicular to the SRR. This magnetic moment then excites a (somewhat weaker) magnetic mode of the corresponding 90°-rotated SRR in the other layer (e.g., SRRs 1<sup>b</sup> and 2<sup>f</sup>). The middle section of that 90°-rotated SRR wire then radiates THz radiation with 90°-rotated polarization, causing optical activity.

Short-circuiting of the SRR gaps at high temperatures ( $2.6 \times 10^5$  S m<sup>-1</sup> VO<sub>2</sub> conductivity) transforms the SRRs into continuous rings, which cannot support the magnetic mode. As a result, only electric dipoles consisting of pairs of weak, nonresonant, parallel charge oscillations can be excited in the structure. These electric dipoles, which are oriented parallel to the excitation field, can only reradiate the incident polarization state, causing an achiral response and transmission without polarization change.

Optical activity breaks the degeneracy of the refractive indices for circularly polarized waves of opposite handedness. The difference between the real parts of the refractive indices

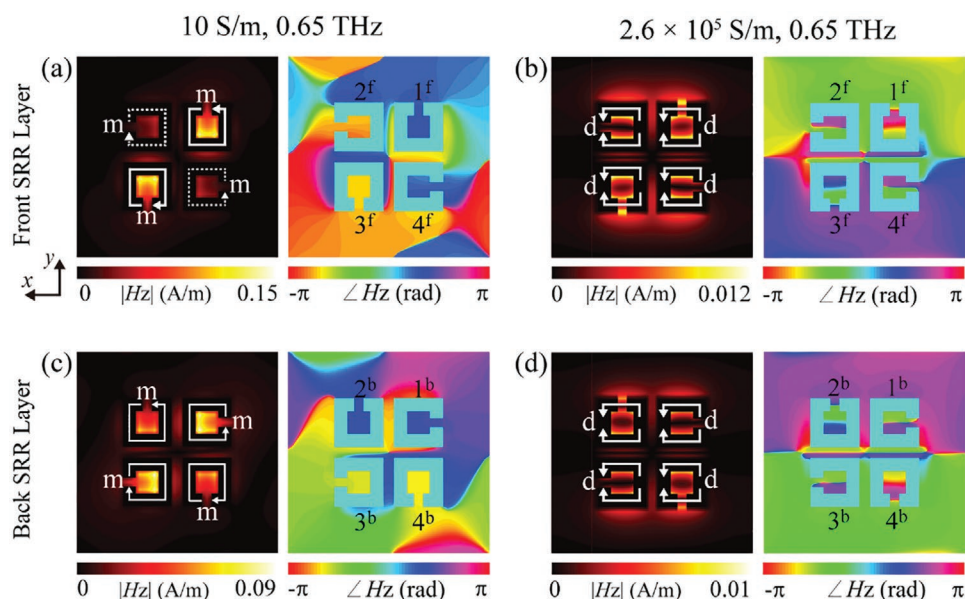


**Figure 5.** Physical mechanism of switchable linear polarization conversion in the hybrid 3D-chiral metamaterial. Modes excited on the a,b) front SRRs layer and c,d) back SRRs layer by an x-polarized 0.65 THz wave normally incident on the front side of the metamaterial when VO<sub>2</sub> is in its a,c) insulating room-temperature phase ( $\sigma = 10 \text{ S m}^{-1}$ ) and b,d) conductive high-temperature phase ( $\sigma = 2.6 \times 10^5 \text{ S m}^{-1}$ ). Amplitude and phase of the magnetic field  $H_z$  are shown within the SRR planes. The instantaneous directions of currents are marked by white lines with arrows. The currents correspond to magnetic and electric dipoles, **m** and **d**, for low and high VO<sub>2</sub> conductivity, respectively. The front and back split rings are labeled 1<sup>f</sup> to 4<sup>f</sup> and 1<sup>b</sup> to 4<sup>b</sup>, respectively.

for LCP and RCP is proportional to circular birefringence, while the difference between the imaginary parts of the refractive indices is linked to circular dichroism. Therefore, metamaterials with strong circular birefringence can exhibit a negative refractive index for one circular polarization. Retrieval of the effective refractive indices<sup>[15,16,29–31]</sup> of the 3D-chiral metamaterial from our simulations reveals negative values around the metamaterial's 0.65 THz resonance when VO<sub>2</sub> is in the dielectric phase, see Figure S1 (Supporting Information). Around the resonance, the refractive indices are strongly dependent on the conductivity of VO<sub>2</sub>. For example, at a frequency of 0.63 THz the real part of the refractive index for RCP increases from  $-5.7$  via zero to  $+3.1$ , whereas the refractive index for LCP reduces from  $+4.8$  to  $+3.1$  as VO<sub>2</sub> transitions from insulating to metallic, see **Figure 6a**. Similarly dramatic switching of the refractive

index for LCP from strongly negative, via zero to positive occurs at a frequency of 0.66 THz, see **Figure 6b**. In all cases, the refractive indices for RCP and LCP converge as optical activity vanishes when the metamaterial is heated to its achiral high-temperature state. Thus, the dielectric-to-metal phase transition of vanadium dioxide enables dynamic control over the refractive indices for circularly polarized THz waves, where the real part can be tuned from negative via zero to positive values.

Despite qualitative agreement, we note that resonances and associated chiral effects are generally weaker in our experiments than in our simulations. This may be because of fabrication inaccuracies and larger losses in the experimental structure. The magnitude of refractive index changes in our experiments can be estimated from the measured circular birefringence of up to  $67^\circ$  at 0.665 THz (**Figure 3d**). Considering the metamaterial

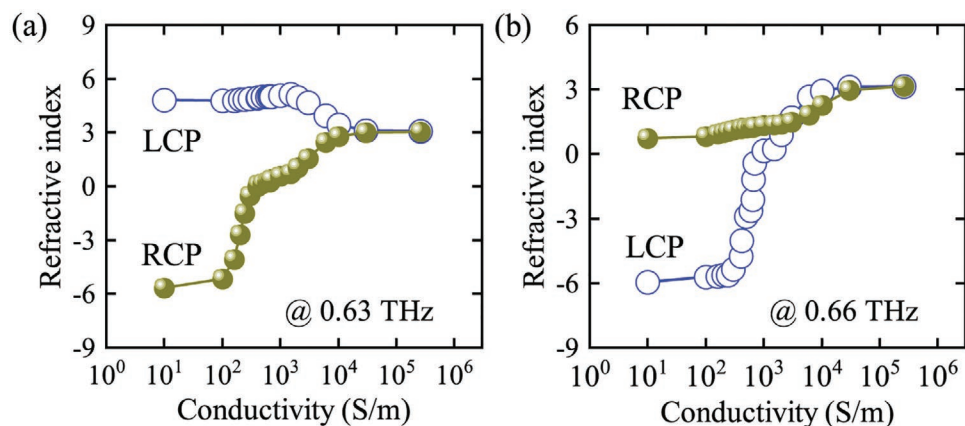


**Figure 6.** a,b) Refractive index for RCP and LCP waves at 0.63 and 0.66 THz as a function of VO<sub>2</sub> conductivity according to numerical simulations.

thickness of 33.7  $\mu\text{m}$ , this corresponds to a difference of 2.5 between the real parts of the refractive indices for LCP and RCP at room temperature, which vanishes when the metamaterial is heated. It follows that the temperature-controlled refractive index changes in our experiments exceed 1 refractive index unit.

While we observe very large chiral effects from just two layers of mutually twisted gold resonators, we note that even stronger effects may be expected from an increased number of layers of mutually twisted resonators.<sup>[15,32]</sup> Furthermore, our metamaterial structure is quite sparse, with clusters of resonators separated by significant gaps. Therefore, a denser structure—with reduced or eliminated gaps between the resonant clusters—may be expected to yield enhanced chiral effects.

In comparison to electromechanical metamaterials,<sup>[17–21]</sup> control of chirality and its manifestations through a phase transition has the fundamental advantage that it does not require any moving parts. Absence of mechanical components simplifies the fabrication and can improve the structure's reliability and speed. While the response time of a mechanical structure is limited by its fundamental mechanical resonance, phase transitions can be very fast. Indeed, THz metamaterials with characteristic length scales of 100  $\mu\text{m}$  or more have sub-MHz mechanical resonances and will respond on milli- to microsecond timescales. In contrast, optical switching of  $\text{VO}_2$  with picosecond optical pulses has been reported.<sup>[33]</sup>

## 4. Conclusion

We have demonstrated temperature control of optical activity and index of refraction in a THz metamaterial. The structure exploits the dielectric-to-metal phase transition of vanadium dioxide to switch between chiral and effectively achiral resonator geometries. This allows its chiral properties, which are exceptionally strong at room temperature, to be tuned and even switched off by heating. We have observed thermal control over circular birefringence, circular dichroism, linear polarization conversion, and refractive index. Indeed, our simulations indicate that the real parts of the refractive indices for circularly polarized waves can be controlled from negative via zero to positive values. The metamaterial's chiral response at low temperatures has been traced to magnetic dipole excitations, which couple between different layers of the 3D-chiral metamaterial. Its achiral response at high temperatures has been explained by electric dipole excitations. Chiral phase change metamaterials like the one presented here may find applications in active polarization control as tunable polarization rotators, switchable circular polarizers, and tunable polarization-selective spectral filters.

## Supporting Information

Supporting Information is available from the Wiley Online Library or from the author.

## Acknowledgements

This work was supported by the National Science Foundation of China (Grant Nos. 61935015, 61875150, and 62025504), the Tianjin Municipal

Fund for Distinguished Young Scholars (18JCQJC45600), and the UK's Engineering and Physical Sciences Research Council (Grant No. EP/M009122/1).

## Conflict of Interest

The authors declare no conflict of interest.

## Author Contributions

M.L. conducted the experiments and simulations. M.L., H.L., C.-H.Z., C.-W.Z., and B.-B.J. fabricated the metamaterial structures. M.L., E.P., S.-X.L., Q.X., X.-Q.Z., J.-G.H., and W.-L.Z. interpreted the results. M.L. and E.P. wrote the manuscript. E.P., J.-G.H., and W.-L.Z. supervised the project. E.P. proposed the project.

## Data Availability Statement

The data that support the findings of this study are openly available in the University of Southampton ePrints research repository at <https://doi.org/10.5258/SOTON/D1646>, reference number [34].

## Keywords

active control, chirality, metamaterials, negative refractive index, optical activity, phase transition

Received: November 29, 2020

Revised: January 7, 2021

Published online: February 3, 2021

- [1] F. J. D. Arago, *Mémoires de la classe des sciences mathématiques et physiques de l'Institut Impérial de France*, 1st part 1811, pp. 93–134.
- [2] L. Pasteur, *Ann. Chim. Phys.* **1850**, 28, 56.
- [3] C. W. Smith, D. G. Gisser, M. Young, S. R. Powers, *Appl. Phys. Lett.* **1974**, 24, 453.
- [4] H. Goto, K. Akagi, *Angew. Chem.* **2005**, 117, 4396.
- [5] M. Faraday, in *Faraday's Diary*, Vol. 4 (Ed: T. Martin), George Bell and Sons, London, UK **1933**.
- [6] K. Aizu, *Phys. Rev.* **1964**, 133, A1584.
- [7] N. I. Zheludev, *Sov. Phys. Cryst.* **1965**, 9, 418.
- [8] S. A. Akhmanov, B. V. Zhdanov, N. I. Zheludev, N. I. Kovrigin, V. I. Kuznetsov, *JETP Lett.* **1979**, 29, 264.
- [9] E. Plum, V. A. Fedotov, A. S. Schwanecke, N. I. Zheludev, Y. Chen, *Appl. Phys. Lett.* **2007**, 90, 223113.
- [10] N. Liu, H. Liu, S. Zhu, H. Giessen, *Nat. Photonics* **2009**, 3, 157.
- [11] Y. Cui, L. Kang, S. Lan, S. Rodrigues, W. Cai, *Nano Lett.* **2014**, 14, 1021.
- [12] M. Esposito, V. Tasco, F. Todisco, M. Cuscuna, A. Benedetti, D. Sanvitto, A. Passaseo, *Nat. Commun.* **2015**, 6, 6484.
- [13] M. Hentschel, M. Schaferling, X. Y. Duan, H. Giessen, N. Liu, *Sci. Adv.* **2017**, 3, e1602735.
- [14] I. Fernandez-Corbaton, C. Rockstuhl, P. Ziemke, P. Gumbsch, A. Albiez, R. Schwaiger, T. Frenzel, M. Kadic, M. Wegener, *Adv. Mater.* **2019**, 31, e1807742.
- [15] E. Plum, J. Zhou, J. Dong, V. A. Fedotov, T. Koschny, C. M. Soukoulis, N. I. Zheludev, *Phys. Rev. B* **2009**, 79, 035407.
- [16] S. Zhang, Y. S. Park, J. Li, X. Lu, W. Zhang, X. Zhang, *Phys. Rev. Lett.* **2009**, 102, 023901.

- [17] T. Kan, A. Isozaki, N. Kanda, N. Nemoto, K. Konishi, H. Takahashi, M. Kuwata-Gonokami, K. Matsumoto, I. Shimoyama, *Nat. Commun.* **2015**, *6*, 8422.
- [18] T. Kan, A. Isozaki, N. Kanda, N. Nemoto, K. Konishi, M. Kuwata-Gonokami, K. Matsumoto, I. Shimoyama, *Appl. Phys. Lett.* **2013**, *102*, 221906.
- [19] L. Cong, P. Pitchappa, N. Wang, R. Singh, *Research* **2019**, 7084251.
- [20] W. J. Choi, G. Cheng, Z. Huang, S. Zhang, T. B. Norris, N. A. Kotov, *Nat. Mater.* **2019**, *18*, 820.
- [21] Q. Zhang, E. Plum, J. Y. Ou, H. Pi, J. Li, K. F. MacDonald, N. I. Zheludev, *Adv. Opt. Mater.* **2020**, 2001826.
- [22] M. Liu, Q. Xu, X. Chen, E. Plum, H. Li, X. Zhang, C. Zhang, C. Zou, J. Han, W. Zhang, *Sci. Rep.* **2019**, *9*, 4097.
- [23] M. Liu, E. Plum, H. Li, S. Duan, S. Li, Q. Xu, X. Zhang, C. Zhang, C. Zou, B. Jin, J. Han, W. Zhang, *Adv. Opt. Mater.* **2020**, *8*, 1901572.
- [24] Q. Y. Wen, H. W. Zhang, Q. H. Yang, Y. S. Xie, K. Chen, Y. L. Liu, *Appl. Phys. Lett.* **2010**, *97*, 021111.
- [25] T. Driscoll, S. Palit, M. M. Qazilbash, M. Brehm, F. Keilmann, B.-G. Chae, S.-J. Yun, H.-T. Kim, S. Y. Cho, N. M. Jokerst, D. R. Smith, D. N. Basov, *Appl. Phys. Lett.* **2008**, *93*, 024101.
- [26] H. Cai, S. Chen, C. Zou, Q. Huang, Y. Liu, X. Hu, Z. Fu, Y. Zhao, H. He, Y. Lu, *Adv. Opt. Mater.* **2018**, *6*, 1800257.
- [27] Y. H. Zhu, Y. Zhao, M. Holtz, Z. Y. Fan, A. A. Bernussi, *J. Opt. Soc. Am. B* **2012**, *29*, 2373.
- [28] Y. Zhu, S. Vegesna, Y. Zhao, V. Kuryatkov, M. Holtz, Z. Fan, M. Saed, A. A. Bernussi, *Opt. Lett.* **2013**, *38*, 2382.
- [29] X. Xiong, W. H. Sun, Y. J. Bao, M. Wang, R. W. Peng, C. Sun, X. Lu, J. Shao, Z. F. Li, N. B. Ming, *Phys. Rev. B* **2010**, *81*, 075119.
- [30] R. K. Zhao, T. Koschny, C. M. Soukoulis, *Opt. Express* **2010**, *18*, 14553.
- [31] Z. Li, R. Zhao, T. Koschny, M. Kafesaki, K. B. Alici, E. Colak, H. Caglayan, E. Ozbay, C. M. Soukoulis, *Appl. Phys. Lett.* **2010**, *97*, 081901.
- [32] Y. Zhao, M. Belkin, A. Alu, *Nat. Commun.* **2012**, *3*, 870.
- [33] O. L. Muskens, L. Bergamini, Y. Wang, J. M. Gaskell, N. Zabala, C. H. de Groot, D. W. Sheel, J. Aizpurua, *Light: Sci. Appl.* **2016**, *5*, e16173.
- [34] M. Liu, E. Plum, H. Li, S. Li, Q. Xu, X. Zhang, C. Zhang, C. Zou, B. Jin, J. Han, W. Zhang, University of Southampton ePrints research repository, <https://doi.org/10.5258/SOTON/D1646>.